Chapter 1

Introduction

1.1 Interstellar clouds

The first indication that the region between the stars may not be empty came through the spectroscopic observations of stars in the early part of this century. While doing spectroscopy of a binary system of stars **Hartman** (1904) noticed absorption lines due to neutral sodium and singly ionised calcium which were stationary in wavelength during the various orbital phases of the binary. This led him to the brilliant conjecture that these absorption lines must be due to gas present in interstellar space. The profound implications of this were overlooked till the late 1930s, with the rare exception of Eddington who devoted the last chapter of his celebrated book on the Internal Constitution of Stars to interstellar matter. The observations of reddening of open clusters by **Trumpler** (1930) clearly established the presence of clouds of ***dust*** in the interstellar space. Many of these clouds appear as dark patches of obscuration in large optical photographs since they block visible radiation from stars behind them. There have been many attempts to catalogue these dark clouds sometimes also called "dark nebulae" [Lundmark and Melotte (1926), **Barnard** (1927), Khavtassi (1960), **Lynds** (1962), Feitzinger and Stuwe (1984), **Hartley** et al. (1986)]. But the concept of the dust being associated with gas clouds is relatively recent.

The major breakthrough in our understanding of the global distribution of matter in the interstellar space came with the discovery of the 21 cm line of hydrogen. Extensive observations have revealed that the interstellar medium as seen in neutral hydrogen consists of cold diffuse clouds ($T \sim 80K$ and $n \sim 20cm^{-3}$) in pressure equilibrium with a widespread warm intercloud medium ($T \sim 6000K$, $n \sim 0.1cm^{-3}$) (Radhakrishnan et al., 1972).

The presence of molecules in interstellar space was known even before the discovery of neutral hydrogen. The narrow absorption features of CN, CH and

CH^+ were recognized in the ultraviolet spectra towards stars. In an important paper Townes (1957) had listed the wavelengths of many simple molecules that could be observed in the microwave spectra. However, it was not until the mid-1960s that astronomers realized that a major fraction of the mass of the interstellar medium was in molecular form, and that the dark clouds of obscuration were in fact molecular clouds. This realization had to wait till the discovery of carbon monoxide in interstellar space (Wilson et al., 1971). Since the hydrogen molecule has no permanent dipole moment $\Delta J = \pm 1$ rotational transitions are forbidden. The other molecular species (such as carbon monoxide) although present only in small quantities do not suffer from this selection rule. During the 1970s major large scale surveys of the Galaxy were undertaken using the rotational lines of ^{12}CO and ^{13}CO and a picture of the distribution of molecular gas in the interstellar medium emerged. It is well established that most of the molecular hydrogen is concentrated in a small number of Giant Molecular Clouds. These clouds are much colder (≤ 35 K) than their HI counterparts. There are also numerous smaller molecular clouds, and the dark clouds which form the subject matter of this thesis, largely belong to this category. Interestingly, the composition of interstellar clouds seems to be either largely atomic or largely molecular. As a'general rule, the atomic clouds constitute a larger fraction in the outer Galaxy while the molecular clouds are dominant in the inner Galaxy. It is also established that the molecular clouds - both large and small - are the sites of active star formation.

1.2 The motions of clouds

In the absence of any perturbation the clouds will be in circular motion around the centre of the Galaxy. But the formation of associations or groups of stars, particularly the more massive O and B stars, has' a significant effect on the motions of these interstellar clouds. The ionising radiation from these stars, their stellar winds during the main sequence phase, and the final supernova explosions represent major sources of energy and momentum to the interstellar medium. Separately or together, these impart systematic motions to the interstellar clouds. There is growing evidence both in the Galaxy and in the Large Magellanic Cloud that the numerous ***shells*** and ***supershells*** that have been discovered may be large cavities in the interstellar medium excavated by the combined effect of the ionising radiation, stellar wind, and supernova activity in O-B associations.

In course of time, these clouds which have acquired a systematic velocity over and above their circular motion will collide with each other, and after a number of such collisions their systematic motion will get randomised. These random motions of clouds have several important consequences. For example, Spitzer and Schwarzschild (1951) have suggested that the observed velocity dispersion and the resultant scale height of the long- lived low mass stars (as well as white dwarfs and neutron stars) may be the result of gravitational encounters between these stars

and the interstellar clouds. But for the fluctuating component of gravitational potential to be significant, clouds with masses in the range $\sim 10^5$ to $10^6 M_\odot$ must have random velocities $\sim$ 6-10 kms^{-1} (Stark and Blitz, 1978). These peculiar motions of the clouds may also be responsible for the formation of giant clouds through cloud-cloud collisions (Kwan, 1979). Thus a detailed knowledge of the distribution of random velocities and its dispersion is of considerable interest. Stark (1984) has concluded from a study of small molecular clouds towards the anticentre direction that the dispersion in their velocities is ~ 9 kms^{-1}. But neutral hydrogen clouds show a much smaller dispersion. For example, from 21 cm observations towards the galactic centre Radhakrishnan and Srinivasan (1980) have shown that the peculiar velocities of HI clouds is well fit by a Gaussian with a dispersion ~ 5 kms^{-1}. The discrepancy between the two values mentioned above needs to be reconciled, and we shall comment upon the velocity dispersion of the local molecular clouds later in this thesis.

1.3 Gould's Belt

The solar neighbourhood appears to be inside an expanding cavity (Figure 1.1). The local system of O-B stars are apparently confined to a plane inclined to the galactic disc at an angle of $\sim 18°$. This 'belt' of stars was first noticed by William Herschell, and later John Herschell and others devoted some attention to it. However, it was Gould who undertook the first systematic observational study of this distribution of stars which hence has come to be named after him (Gould, 1879). The initial studies were necessarily restricted to its morphology and its relation to the galactic disc. Kinematical studies had to wait till galactic differential rotation had been firmly established. Oort (1927) noted that the stars in the local system appear to have a positive residual velocity ~ 5 kms^{-1} after correcting for differential rotation, and allowing for some peculiar velocities. The next major advance in the kinematical analysis of stellar velocities came with the concept of 'expanding local groups' (Blaauw, 1956). This idea was used by Bonneau (1964) who analyzed Eggen's stellar data (1961), from which he deduced an expansion age of the system of $\sim$ 40 Myrs. Subsequent to this there have been many studies of the Gould's belt system of stars [Lesh (1968), Stothers and Frogel (1974), Frogel and Stothers (1977), Westin (1985), Cameron and Torra (1990)].

The study of gas associated with Gould's belt is more recent. The earliest study was that of Lindblad (1967) who observed the HI gas associated with the system of expanding stars. Later Lindblad et al. (1973) studied the kinematics of the local HI gas and concluded that this gas has a ring-like geometry, and that it is expanding at ~ 3.5 kms^{-1}, with an expansion age $\sim$ 60 Myrs. This model was further improved and refined by Olano (1982).

The first systematic study of the local molecular clouds, their distribution and kinematics, and their possible association with Gould's belt is due to Taylor et al.

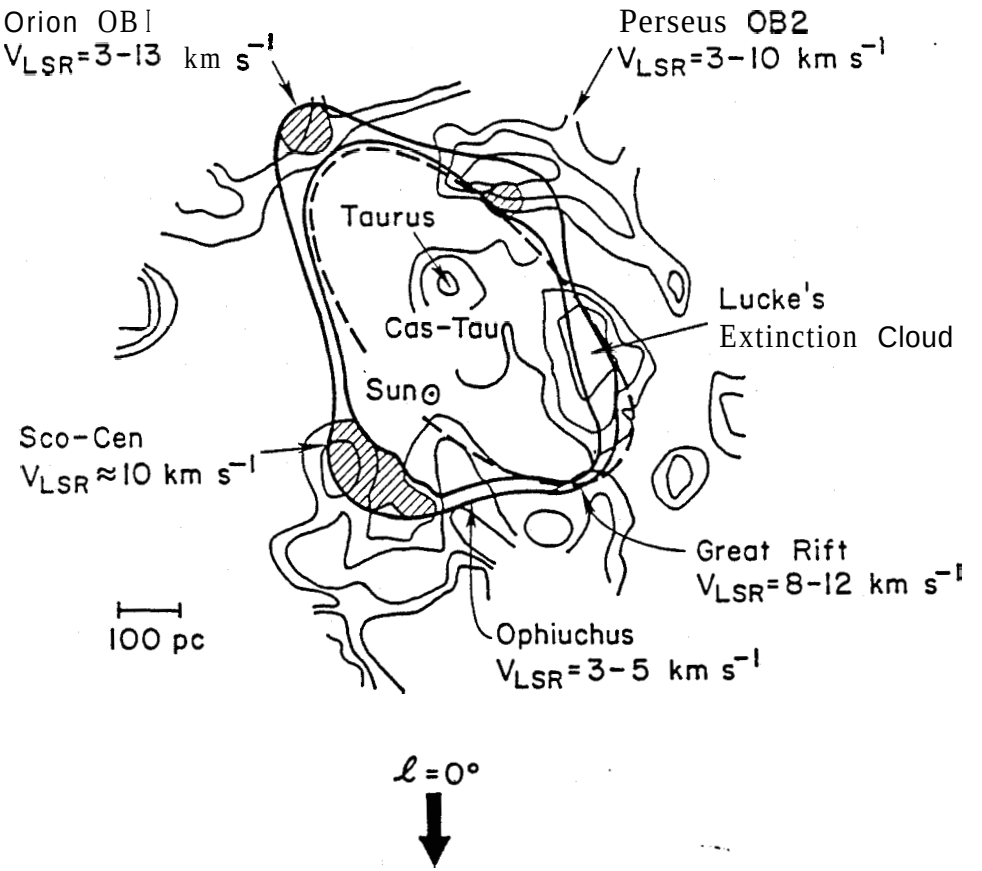

Fig.1.1 : The giant local cavity around the Sun. Prominent OB associations in Gould's belt **viz.** Orion, Perseus and Scorpio-Centaurus are shown. Dashed line is the Lindblad's expanding ring model (Lindblad et al., 1973) for the local HI gas. The contours show the distribution of local dust complexes determined from interstellar reddening (Lucke, 1978). The figure is from Elmegreen, 1991.

(1987). Using a simple proximity criterion (explained in Chapter 5) they separated the population of the northern dark clouds into two subgroups – one belonging to the galactic disc and the other confined to an inclined plane called the Gould's belt plane. They found that the clouds identified with the Gould's belt plane showed evidence for expansion, but they could not make a quantitative study for lack of reliable distance estimates to these clouds.

1.4 Basic objectives of the thesis

This thesis is devoted to a detailed kinematic study of the local population of dark clouds, both northern as well as southern. The main motivation for embarking on this study is the following: Taylor et al. (1987) have studied the motions of only the northern molecular clouds. Although they were able to conclude that this population was in a state of expansion, they could not fit the molecular cloud data to the expanding "ring model' suggested by HI studies. Nor were they able to derive an alternative model for the expanding molecular clouds. The clouds studied by Taylor et al. were distributed in the longitude range $0 < l < 220°$. We felt that extending these observations to the rest of the longitude range i.e. $220° < 1 < 360°$ might enable one to construct a model for the kinematics of the dark clouds. There were also other reasons for studying the southern clouds. For example, whereas Kerr et al. (1981) found that "Lindblad's feature *A*" which delineated the Gould's belt in the northern sky was also present in the third quadrant up to $l \sim 236°$, May et al. (1988) found that there was no evidence for a corresponding feature traced by molecular clouds in their southern CO survey. Thus it was important to make an independent study of the southern dark clouds to confirm whether there was a molecular counterpart to the Gould's belt and the associated HI in the southern Galaxy as well. Towards this end we have observed a large population of southern dark clouds taken from the catalogue of Feitzinger and Stuwe (1984), most of them of opacity class > 2. In addition, we have observed some of the northern clouds taken from the catalogue of Taylor et al. (1987) to study the average physical conditions prevailing in them.

In Chapter 2, we describe the telescope used, the observational procedure and the data reduction. We also estimate the measurement errors in the various quantities. Three appendices given at the end of this thesis pertain to this chapter. Appendix A deals with the procedure of calibrating the data. In Appendix B we present the catalogues of the observed sources and their derived properties. Some spectra with interesting line profiles are given in Appendix C.

Since we have observed close to the centres of a large number of clouds distributed over all the longitudes, and over a wide latitude range, this population is ideally suited for a study of the average physical conditions prevailing in the local clouds. While a detailed study is outside the scope of this thesis, we nevertheless present some statistical distributions of the derived parameters in Chapter 3,

pointing out what we consider to be some interesting trends.

Chapter 4 is devoted to a detailed kinematical analysis of the local dark clouds. The analysis is broadly divided into three parts: Part 1 deals with the analysis of the clouds in what refer to as the null directions, i.e. the directions in which contributions due to the galactic differential rotation to the radial velocities of the nearby clouds are less than the rms velocity dispersion. In the second part we analyse the radial velocities of a set of clouds for which reasonably good distance estimates exist. Two subsets of clouds are analysed: (1) Clouds with associated reflection nebulae (2) Clouds identified from the composite CO survey. Finally, in the third part we analyse the radial velocities of the general population of clouds using statistical methods and derive their expansion velocity, dispersion in their velocities about this mean expansion, as well as their spatial distribution. Appendix D given at the end of the thesis summarises the results of the simulations described in this Chapter.

In Chapter 5 we compare our results derived from the analysis presented in Chapter 4 with the conclusions arrived at earlier from CO, neutral hydrogen, and optical studies. We also comment upon some of the earlier speculations regarding the origin of the expanding local system of stars and gas.

Chapter 6 deals with the study of a particular cloud L1616. This cometary cloud occuring in the Orion region was suspected to have a high star formation efficiency (SFE). In order to verify this, we obtained detailed maps of this cloud in CO and its isotopic species. In this Chapter, we present these maps and argue that the SFE is indeed high and that the star formation might have been externally triggered by ϵ Orionis.

References

Barnard, E.E. 1927, A *Photographic Atlas* of Selected Regions of the Milky Way, Carnegie Institution of Washington, D.C..

Blaauw, A. 1956, *Astrophys.J.*, 123, 408.

Bonneau, M. 1964, *J.Obs.*, 47, 251.

Cameron, F., Torra, J. 1990, *Astr.Astrophys.*, 241, 57.

Eggen, O.J. 1961, *R.Obs.Bull.* No.41.

Elmegreen,B.G. 1991, in The galactic interstellar medium, eds. W.B. Burton, B.G. Elmegreen, R.Genzel (Saas-Fee advanced course 21), 164.

Feitzinger, J.V. and Stuwe, J.A. 1984, *Astr.Astrophys.Suppl.*, 58, 365.

Frogel, J.A., Stothers, R. 1977, *Astron.J.*, 82, 890.

Gould, B.A. 1879, Uranometria Argentina (P.E.Coni, Buenos Aires) 335.

Hartley, M., Manchester, R.R., Smith, R.M., Trittou, S.B.,Goss, W.M. 1986, Astr. *Astrophys. Suppl.*, 63, 27.

Rartman, J.F. 1904, *Astrophys.J.*, 19, 268.

Kerr, F.J., Bowers, P.F., Hendrson, A.P. 1981, *Astr.Astrophys.Suppl.*, 44, 63.

Khavtassi, D.Sh. 1960, Atlas of Galactic Dark Nebulae (Acad.Sci.Georgian SSR, Tiflis).

Kwan, J. 1979, *Astrophys.J.*, 229, 567.

Lesh, J.R. 1968, *Astrophys.J.Suppl.*, 17, 371.

Lindblad, P.O., Grape, K., Sandqvist, Aa., Schober, J. 1973, *Astr.Astrophys.*, 24, 309.

Lindblad, P.O. 1967, *Bull.Astron.Inst.Neth.*, **19**, 34.

Lucke P.B. 1978, *Astr.Astrophys.*, 64, 367.

Lundmark K., Melotte, P.J. 1926, Uppsala *Medd.*No.12.

Lynds, B.T. 1962, *Astrophys.J.Suppl.*, 7, 1.

May, J., Murphy, D.C., Thaddeus, P. 1988, *Astr.Astrophys.Suppl.*, 73, 51.

Olano, C.A. 1982, *Astr.Astrophys.*, 112, 195.

Oort, J.H. 1927, *Bull.Astron.Inst.Neth.*, 3, 275.

Radhakrishnan, V., Srinivasan G. 1980, *J.Astrophys.Astr.*, **1**, 47.

Radhakrishnan, V., Murray, J.D., Lockhart, P., Whittle, R.P.J. 1972, Astrophys. J. *Suppl.*, 24, 15.

Spitzer, L., Schwarzschild, M. 1951, *Astrophys.J.*, 114, 385.

Stark, A.A., Blitz, L. 1978, *Astrophys.J.(Lett)*, 225, L15.

Stark, A.A. 1984, *Astrophys.J.*, 281, 624.

Stothers, R., Frogel, J.A. 1974, *Astron.J.*, 79, 457.

Taylor, D.K., Dickman, R.L., Scoville, N.Z.1987, *Astrophys.J.*, 315, 104.

Townes, C.H. 1957, in it IAU Symposium No.4, ed.H.C.van de Hulst, Cambridge, 92.

Trumpler, R.J. 1930, *Publ.Astr.Soc.Pacific*, 42, 214.

Westin,T.N.G. 1985, *Astr.Astrophys.Supl.*, 60 ,99.

Wilson, R.W., Jefferts, K.B., Penzias, A.A. 1971, *Astrophys.J.(Letters).*, 161, L43.

Chapter 2

Observations

2.1 Sources

As explained in the previous chapter, the major subject matter of this thesis is the kinematical study of the local population of dark clouds. The only systematic study of the local molecular clouds reported in the literature so far with a view to ascertain their possible association with Gould's belt is that of Taylor et al. (1987). They have compiled a list of highly opaque dark clouds in the longitude range 0° to 240° from a careful inspection of the Palomar Observatory Sky Survey (POSS) prints and obtained radial velocities towards them using the $J = 1 \rightarrow 0$ transition line of carbon monoxide with the 14m antenna of the Five College Radio Astronomy Observatory. However, their catalogue lists only the coordinates, and the LSR velocities of these clouds. Line strengths and widths which are important for the study of the average physical properties, of the local dark clouds have not been listed. Further, they could not observe the southern dark clouds in the longitude range 240° to 360° owing to the inaccessibility of these clouds at their northern site. We have made observations with the 10.4m antenna of the Raman Research Institute meeting both these requirements to a certain extent.

Our primary motive for these observations was to find out if some molecular clouds also trace Gould's belt in the southern galaxy and if they do, whether they also show expansion similar to their northern counterparts. In addition, we intended to study the average physical properties of the local dark clouds.

The observations reported in this chapter consist of ^{12}CO and ^{13}CO surveys of 274 northern clouds and 142 southern clouds. The coordinates of the northern clouds were taken from the catalogue of Taylor et al (1987). No particular criteria were used to choose the clouds to be observed. Whether or not we observed a cloud listed in their catalogue was decided by the availability of telescope time. The clouds from their catalogue were observed primarily to determine their average

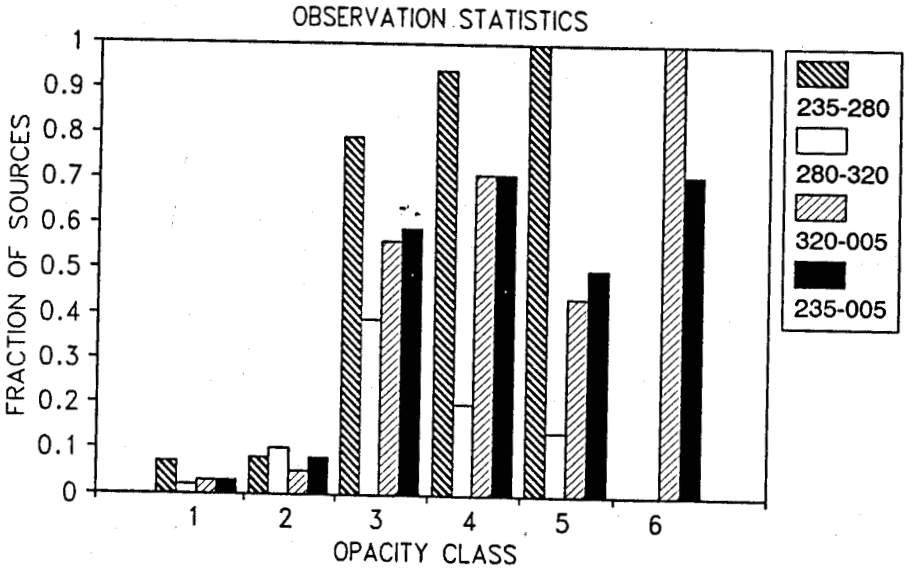

Fig.2.1.a : The distribution of the fraction of southern dark clouds observed as a function of their opacity class.

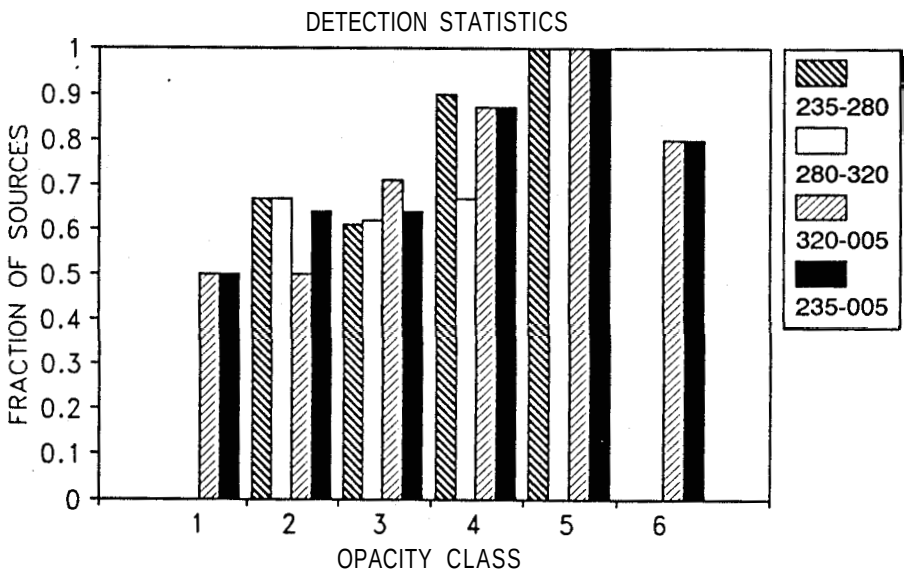

Fig.2.1.b : The fraction of the observed dark clouds actually detected. The legends in boxes indicate the relevant longitude ranges in degrees.

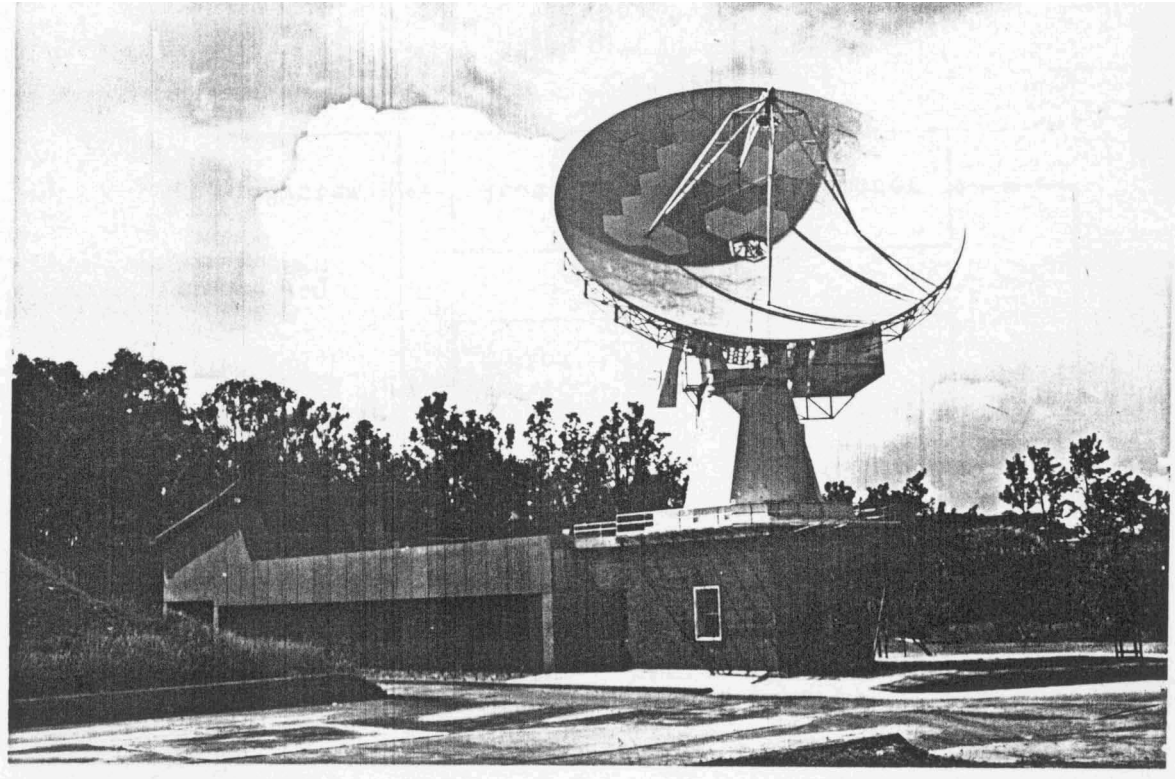

Fig.2.2a: The 10.4 meter millimeter wave telescope at the Raman Research Institute campus, Bangalore. The observations reported in this thesis were made with this telescope.

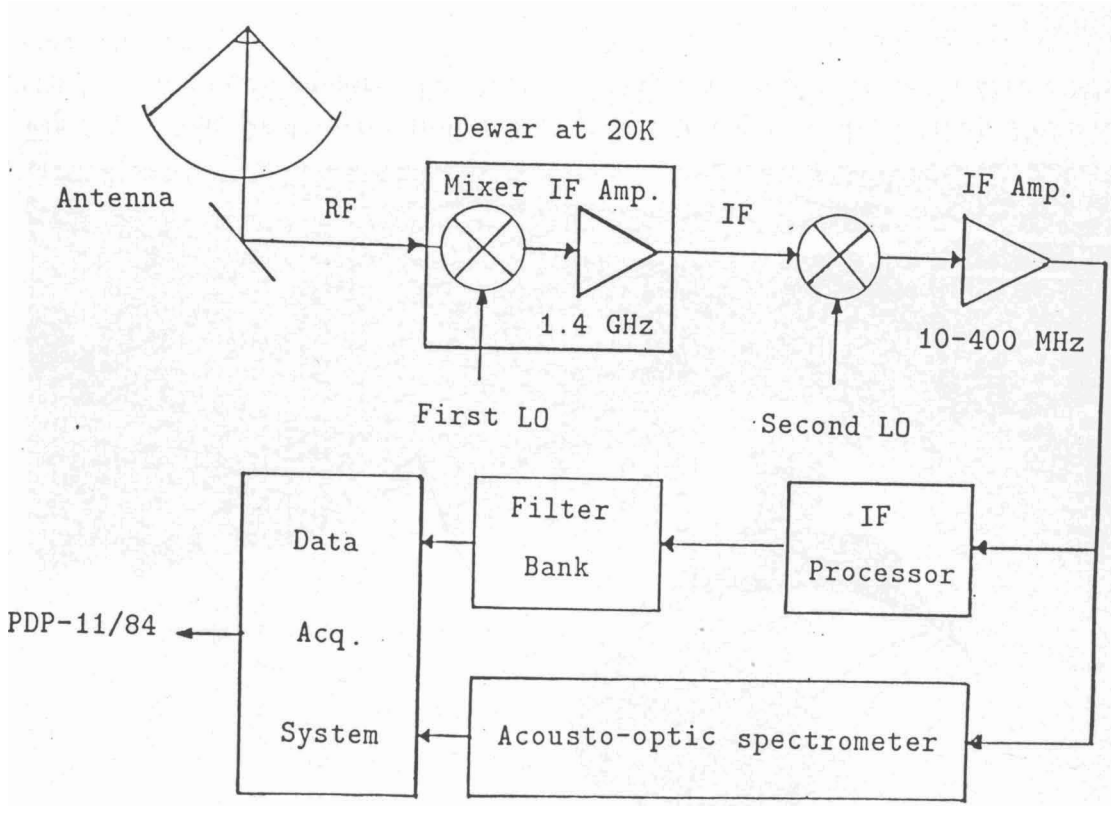

Figure 2.2b A simplified block diagram of the receiver system at the 10.4m telescope.

physical properties. Whenever available, 'we have used the radial velocities listed by Taylor et al.(1987). The southern clouds in the longitude range 240° to 360° were selected from the catalogue of dark nebulae compiled by Feitzinger and Stuwe (1984) from a study of ESO(B) and SERC(J) sky atlas based on opacity class (mostly > 2) and declination. Figure 2.1.a shows a histogram of observational statistics, and 2.1.b shows a histogram of the detection statistics. These are further discussed in the last section of this chapter. Appendix B lists the observed northern clouds, southern clouds, and clouds with associated reflection nebulae.

2.2 Some details of the telescope

All the observations reported in this thesis were done with the 10.4 m millimeter wave telescope at the Raman Research Institute campus in Bangalore (fig.2.2.a). The site is at 930 m above the mean sea level at a latitude of 13°01′ North and longitude of 77°35′ East. The observing season is between November and March, the driest period of the year, with the precipitable water vapour content in the atmosphere $\leq$ 15 mm and the zenith optical depth at 115 GHz $\leq$ 0.25. Over the rest of the year the precipitable water level usually exceeds $\sim$ 23 mm. Reliable measurements for optical depth during the off-season do not exist at 115 GHz. To give an idea, the zenith optical depth at 86 GHz is usually greater than 0.6.

The telescope is a Cassegrain type antenna on the altitude-azimuth mount with the receiver at the Nasmyth focus. The primary is a 10.4 m paraboloid made of hexagonal honeycomb sandwiched aluminium panels, with an RMS surface deviation of $\sim$ 120 microns. The secondary is a hyperboloid of diameter 60 cm with an eccentricity of 1.06. The secondary can be moved in and out along the axis by 5 mm from the mean position to adjust the focus. A tertiary mirror which reflects the beam from the horn onto the secondary can be switched between two positions throwing the beam by a few arc minutes. This mode of observing known as "beam switching" can be used for sources of small angular extent of, say, $<$ 3'.

A schematic of the double side-band (DSB) receiving system used is shown in figure 2.2.b. The first element of the receiver is a 30 K cooled Schottky diode mixer followed by a 30 K cooled low noise GaAs FET amplifier. A commercial Gunn diode oscillator with a tuning range from 80 GHz to 115 GHz is the Local Oscillator. The first intermediate frequency (IF) output is from 1.25 GHz to 165 GHz. This is further down converted to 0 to 400 MHz base-band before being fed to the backends.

Backends in use with sufficient spectral resolution for molecular cloud observations are a 256 channel filter bank with a resolution bandwidth (RBW) of 250 KHz, and a 500 channel Acousto Optic Spectrometer (AOS) with an RBW of 70 KHz. Even though the AOS with its better resolution would have been desirable, we could not use it due to its appreciable lack of gain and frequency stability. Hence for all our observations we have used the filter bank which gives a veloc-

ity resolution of 0.65 km/s and 0.68 km/s at the ^{12}CO and ^{13}CO frequencies, respectively.

The data from the backends are collected and averaged by a dedicated Data Acquisition System which is then transferred to a PDP 11/84 the control computer for header attachment and storage. The data reduction with the PDP 11/84 is usually to get a quick look only. The major part of the reduction was done with a VAX 11/780 computer using a modified version of POPS (People Oriented Parsing Service) package from the National Radio Astronomy Observatory. Table 2.1 surnmarises the important parameters of the telescope and its performance.

Table 2.1 : Telescope Particulars

Parameters		Performance			
Primary dia.	10.4 m	Frequency (GHz)	87	97	114
Primary F/D	0.4	$T_{R,DSB}$ (K)	240	270	280
Secondary dia.	0.6 m	$T_{SYS,DSB}$ (K)	350	-	530
Mount	Altazimuth	Jy/K conversion	72	76	162
Drive per axis	Two DC motors	Beam size (″)	75	65	60
Slew rate	40° /min.	Efficiencies			
Encoders	21 bit (0.6")	Aperture	0.45	0.43	0.2
Surface errors	120μ rms	Main-beam		-	0.6
Control Computer	PDP 11/84	Extended			
Frequency coverage	80-115 GHz	beam (moon)	0.8	-	0.72

2.3 Details of the observational procedure

Observations of the local dark clouds in the two spectral lines ($J = 1 \rightarrow 0$ transitions of ^{12}CO and ^{13}CO) were carried out during the winter of 1991- 92. A pointing model was constructed during the early part of the season using continuum scans of Jupiter obtained in a beam-switched mode. The details of the method of obtaining a pointing model from planet scans are described in Patel (1990). Although Jupiter covers only a restricted track in the sky, from grid-observations of SiO masers the pointing model was found to be reasonably good over all parts of the sky. The reliability of the model was checked by observing Jupiter twice a week. Figure 2.3 shows the distribution of the pointing errors as obtained from this monitoring. It can be seen in the figure that despite an uncorrected d.c offset the pointing errors during our observations were less than 20″ with an rms of $\sim$ 10". The allowed peak to peak tracking error during the observations was $\sim$ 15".

In addition to any line-emission from the clouds, contributions from the receiver, the background, the atmosphere and the sky as well as the d . ~ offsets in the post-detection amplifiers are also present in the spectral channel outputs. The line emission from the dark clouds extend only over a few spectral channels while the other components contribute to all the channels in the observation band. The

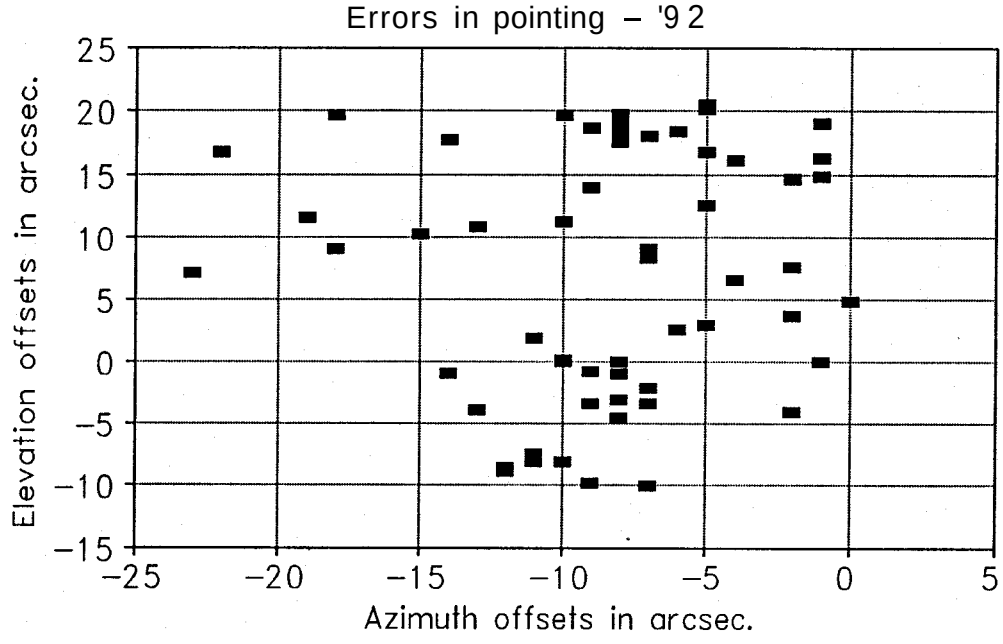

Fig.2.3 : The distribution of pointing errors derived from observations of Jupiter. Notice that there is a residual *dc* error $\sim 10''$ in azimuth, and $\sim 5''$ in elevation. Even if one did not correct for this *dc* offset the residual errors are $\sim 20''$.

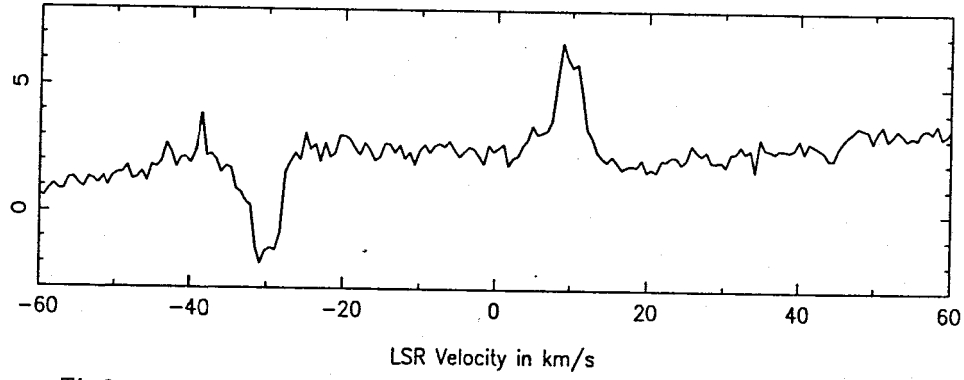

Fig.2.4.a : A typical spectrum obtained by calibrating the difference between the ON and OFF frequency channel outputs.

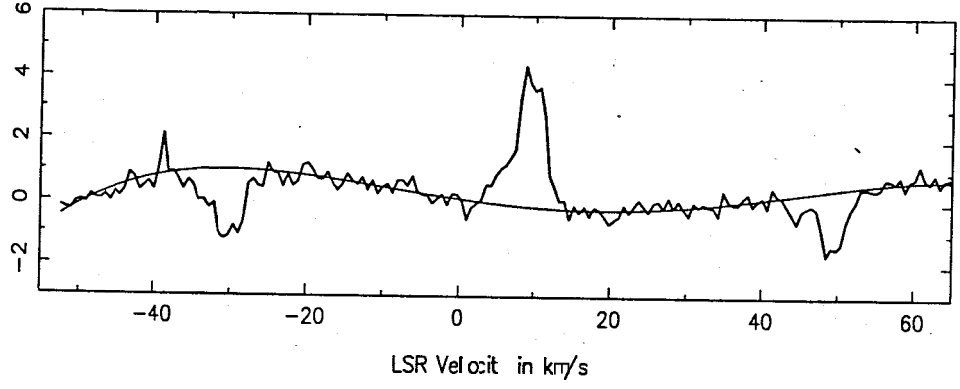

Fig.2.4.b : Switching the frequency results in curved baseline and the negative components. This shows the *folded* spectrum after a third order polynomial fit to the baseline.

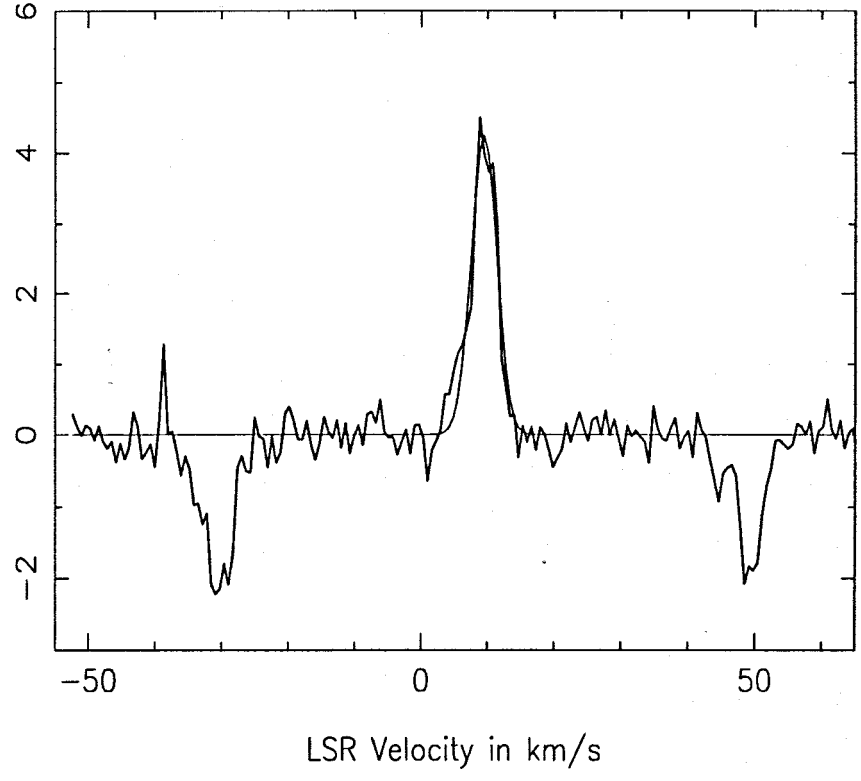

Fig.2.4.c : The Gaussian fit to the spectrum after removing the baseline.

removal of these other components is generally termed as "sky-subtraction". To do this, one needs to obtain two sets of channel output measurements: one on the spectral line and the other off the line or with the line shifted in channel number. Also, these measurements need to be done fast enough so that the receiver gain can be assumed to remain constant.

This is achieved by switching some appropriate element of the system. Switching can be between either on-source and off-source positions or on-line and off-line frequencies. In the latter method known as frequency switching, the L.O. frequency is switched between two nearby values. This shifts the line to a neighbouring set of channels during the OFF period rather than shifting it out entirely. Hence it is twice more time-efficient than switching between positions which requires observing a source-free position for half the time. However, when one switches the L.O. frequency the receiver characteristics are slightly different at the two frequencies. This results in an inexact sky-subtraction leading to curved baselines. If one is observing narrow lines rather than low level extended spectral features this baseline curvature is not a handicap. Hence we adopted the frequency switching mode for all our observations. In any case, beam switching was ruled out because of the extended nature of the sources since the available throw was only ~ 120". Position switching could not be used as the receiver is not stable enough.

The first harmonic of the baseline ripple at the RRI telescope has a period of 15.25 MHz. The ripple is caused by the resonant "cavity" formed by the receiver horn and the secondary seperated by ~ 10 m. By choosing the difference between the ON and OFF frequencies to be equal to the period (15.25 MHz), most of the ripple is subtracted out in the final spectra. The switching rate was 2 Hz.

The spectral channel outputs have also to be converted to normalised units by calibrating against some standard noise source. This was done by observing an ambient temperature absorber for 20 seconds once every 300 seconds. Appendix A details the calibration procedure. During the observations reported here the zenith atmospheric optical depth measured by tipping the telescope was typically 0.25. The elevations of the sources at the time of observation ranged from 20° to 85°. The telluric CO line was seen in a few spectra. These lines were easy to identify as they always appear at an LSR velocity equal to the negative of the LSR correction applied. .

A typical spectrum with its baseline is shown in figure 2.4.a after sky- subtraction and calibration. The two spectral features seen are from the ON and OFF frequency observations. This spectrum is shifted, inverted and averaged with the unshifted one to get the final spectrum. A third order polynomial is fitted to this to remove baseline curvature as shown in figure 2.4.b. The resultant spectrum with its gaussian fit is shown in figure 2.4.c.

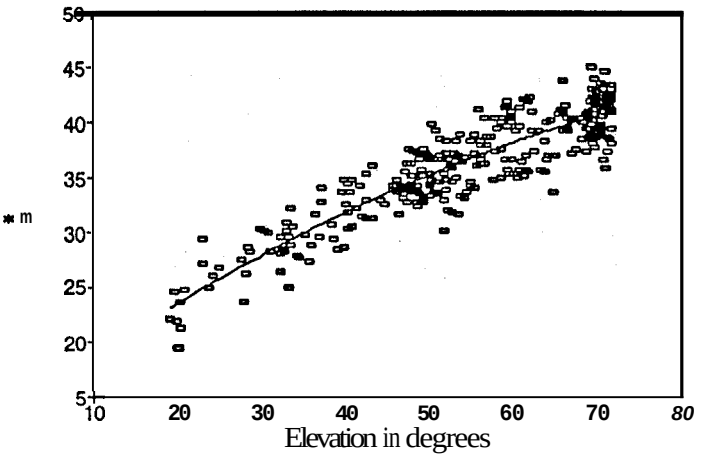

Fig.2.5.a : ^{12}CO line strength (T_a^*) at a standard position on the Orion Molecular Cloud plotted against the elevation of the source at the time of the observation. A second order fit to the elevation dependence of the aperture efficiency of the telescope at 115 GHz is also shown.

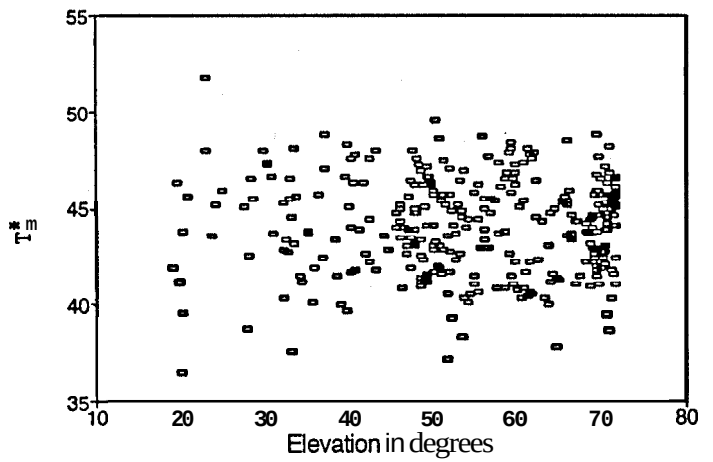

Fig.2.5.b : Antenna temperatures after correcting for the elevation dependence of the aperture efficiency. .

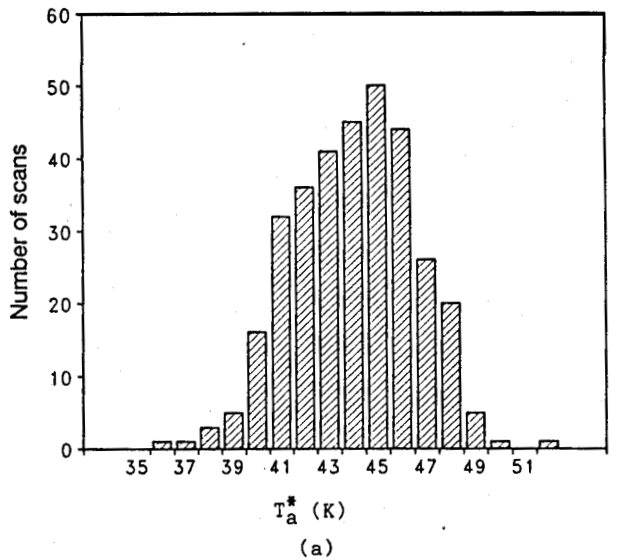

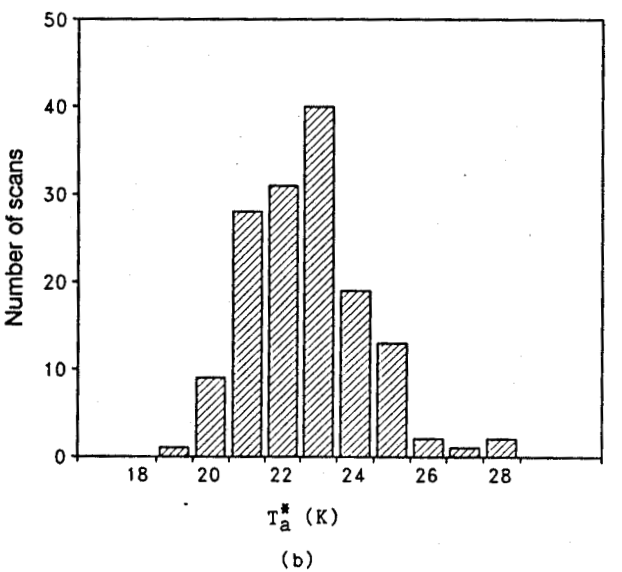

Fig.2.6 : (a) The distribution of the ^{12}CO antenna temperatures at a standard position of the Orion Molecular Cloud after correcting for the elevation dependence of the aperture efficiency. (b) A similar plot for M17SW.

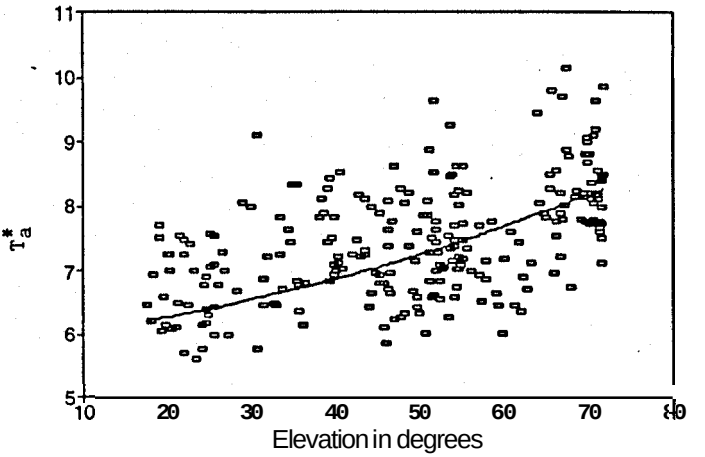

Fig.2.7.a : ^{13}CO line strengths (T_a^*) at a standard position on the Orion Molecular Cloud plotted against the elevation at the time of observation. A second order fit to the elevation dependence of the aperture efficiency at 110 GHz is also shown.

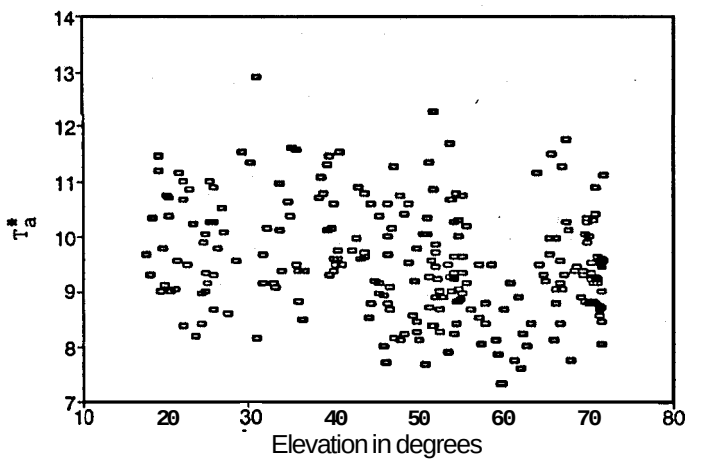

Fig.2.7.b : Antenna temperatures after correcting for the elevation dependence of the aperture efficiency.

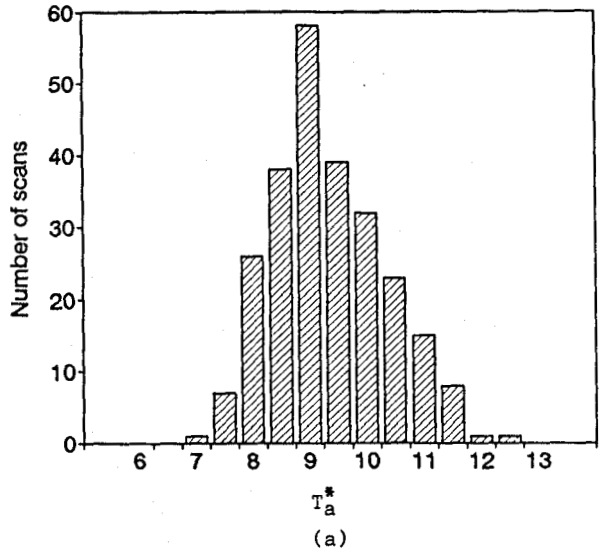

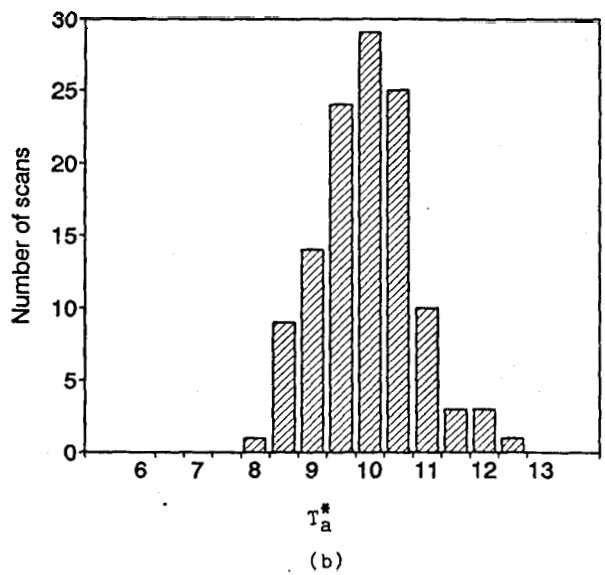

Fig.2.8 : (a) The distribution of ^{13}CO antenna temperatures at a standard position on the Orion Molecular Cloud after correcting for the elevation dependence of the aperture efficiency. (b) A similar plot for M17SW.

2.4 Line strength calibration

In the previous section a brief account of the method of obtaining spectra from raw data was given. To obtain calibrated line strengths the spectra thus obtained have to be further corrected for the aperture efficiency and the forward beam coupling efficiency of the telescope. For this purpose a selected position in each of the following two standard regions viz. the Orion Molecular Cloud (OMC) and M17SW (the south west part of the 17^{th} object in Messier's catalog) were observed two or three times a day throughout the observing season. The data from these calibration sources were subjected to the same procedure outlined in the previous section and the line strengths were obtained. The calibration sources were observed at chosen times so that the entire range of elevations were sampled as much as possible. A plot of the line strengths from OMC as a function of elevation and a parabolic fit are shown in figure 2.5.a. The fit yielded the following correction factor due to the elevation dependence of aperture efficiency:

$$f_{^{12}CO}(EL) = 1/(0.3026 + 0.01268EL - 5.5 \times 10^{-5} EL^2) \quad (2.1)$$

Here EL is the elevation of observation in degrees.

Figure 2.5.b shows the antenna temperature of OMC after correction. Figure 2.6.a shows their distribution. The rms calibration error after correction is $\sim$ 6%. To ensure that this correction works, it was applied on the line- strengths obtained from M17SW. The distribution of the line-strengths after correction is shown in figure 2.6.b. This also has an rms calibration error of $\sim$ 6%, increasing one's confidence in the method. Adopting a similar procedure, the following factor was obtained to correct the ^{13}CO data for the elevation dependence of aperture efficiency:

$$f_{^{13}CO}(EL) = 1/(0.632 - 1.4 \times 10^{-3} EL + 4.44 \times 10^{-5} EL^2) \quad (2.2)$$

Figure 2.7.a shows ^{13}CO OMC data with the fit. The corrected data is shown in figure 2.7.b and its distribution in figure 2.8.a. The distribution of ^{13}CO line strengths from M17SW after correction is shown in figure 2.8.b. The rms calibration error from the OMC data is $\sim$ 10% while from M17SW is $\sim$ 7%. The reason for the worsening of OMC calibration is believed to be due to a substantial fraction of the observations which had to be made in the day-time.

2.5 Reliability of measured velocities

The reliability of the measured velocities was checked in a number of ways. Figure 2.9.a shows the distribution of the differences of velocities measured by us and the corresponding values reported by Taylor et al. (1987) for the subset of clouds taken from their catalogue. The errors are predominantly less than 0.6 km/s. Figure 2.9.b shows the distribution of differences of velocities determined from the ^{12}CO

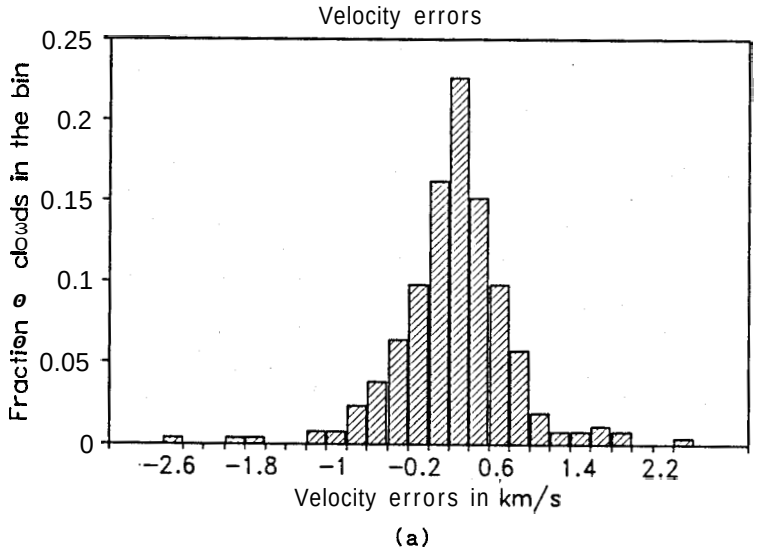

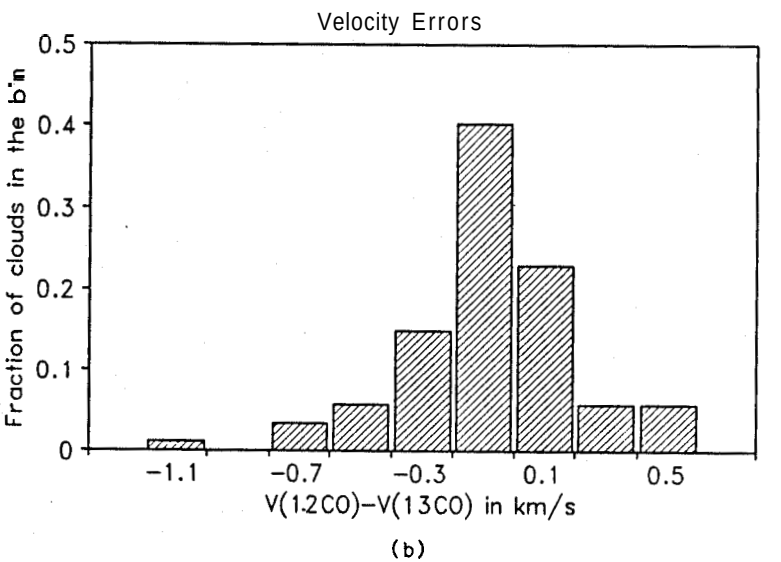

Fig.2.9 : The distribution of the *differences* in velocities of the nothern dark clouds between our measurements and those reported by Taylor et al. (1987) is shown in Fig.(a). The distribution of the *differences* between ^{12}CO and ^{13}CO velocities for clouds in which both the isotopic species were observed by us is shown in Fig.(b).

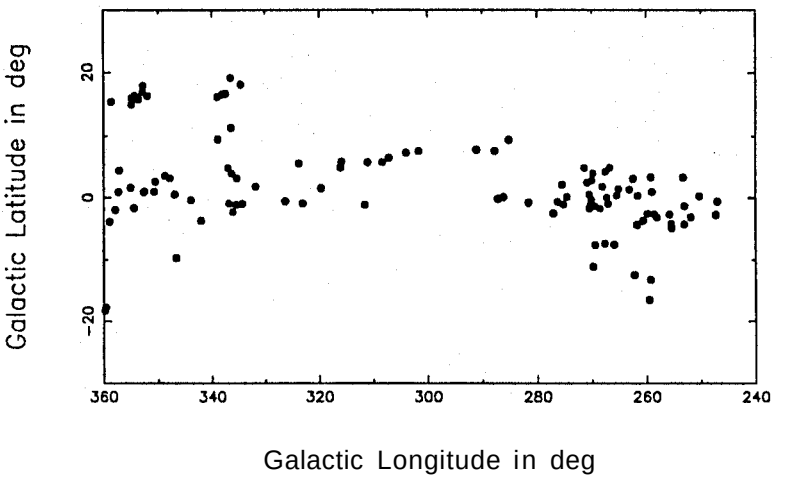

Fig.2.10.a : (a) A plot of the latitude vs longitude of the southern dark clouds detected in our survey.

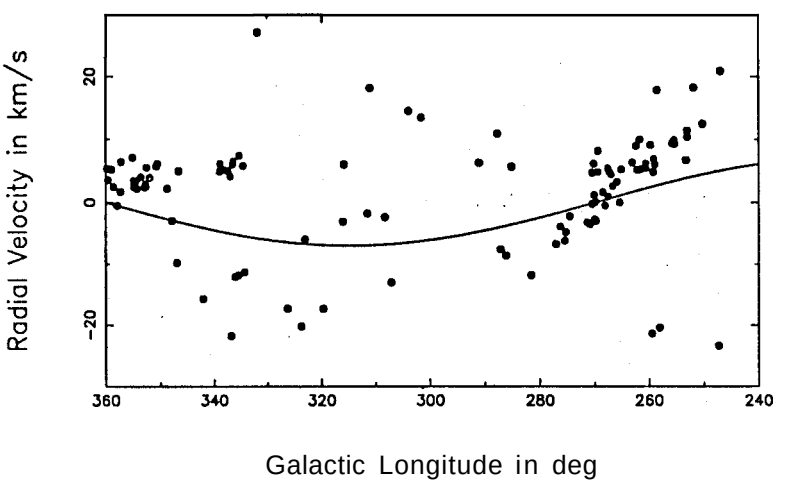

Fig.2.10.b : The radial velocities of the southern dark clouds as a function of their longitudes. The curve is not a fit but the expected behaviour of clouds at an assumed distance of 400 pc from the Sun if their motions were purely due to galactic rotation. (A value of 17.5 km/s/kpc has been assumed for Oort's A constant).

and ^{13}CO spectra of sources for which both the spectra were obtained. This also has a similar rms error of $\sim$ 0.5 km/s. Hence, we conclude that the velocities are reliable to 0.4 $\left(= \frac{0.6}{\sqrt{2}}\right)$ km/s which is close to half of the resolution band-width of the backend used.

2.6 Detection statistics

Table 2.2 lists the number of dark clouds with opacity class 3 or more listed in the catalogue of Feitzinger and Stuwe (1984) in each longitude range and how many were observed and how many among them were detected. Only 30% of the sources in the longitude range 280-320° were accessible from our site. In the other longitude ranges 240-280° and 320-360°, we have observed 85% and 64% of the sources respectively. As mentioned earlier, figure 2.1.a gives a histogram of the observational statistics for each 40 degree longitude intervals, and the net average as a function of opacity class. Figure 2.1.b depicts the detection statistics. Our detection limit was 1.0 K. Failure to detect 20% of the opacity class 6 objects could be due to coordinate errors owing to their small sizes. The reason for non-detection of a slightly larger fraction of opacity class 3 and 4 objects is not clear. Appendix B lists the cloud serial number from the respective catalogues, longitude and latitude of observation, velocity, ^{12}CO line strength, width, rms, ^{13}CO line strength, width and rms for the detected northern clouds, southern clouds, and clouds with associated reflection nebulae, respectively. Sources whose spectra show more than one component have been tabulated separately. The longitude-latitude and latitude-velocity plots of detected southern dark clouds are shown in figure 2.10.a. and 2.10.b, respectively.

Table 2.2 : Observation and detection statistics.

Long. range	Clouds	Observed	Detected	Observed %	Detected %
240° – 280°	80	69	53	86.3	76.8
280° – 320°	57	17	11	29.8	64.7
320° – 360°	99	63	51	63.6	81.0

References

Feitzinger, J.V. and Stuwe, J.A. 1984, *Astr.Astrophys.Suppl.*, **58**, 365

Patel, N.A. 1990, Ph.D.thesis, Indian Institute of Science, Bangalore.

Taylor, D.K., Dickman, R.L., Scoville, N.Z.1987, *Astrophys.J.*, 315, 104.

van den Bergh, S. 1966, *Astron.J.*, 71, 990.